Reconstruction of Missing Data in the Sky using Iterative Harmonic Expansion

Atsushi J. Nishizawa[*]

Kavli Institute for the Physics and Mathematics of the Universe (Kavli IPMU,
WPI), The University of Tokyo, Chiba 277-8583, Japan

Kaiki Taro Inoue

Department of Science and Engineering, Kinki University, Higashi-Osaka, 577-8502, Japan
(Dated: May 1, 2013)

Missing fluctuations in masked regions in the sky can be reconstructed from fluctuations in the surrounding unmasked regions if they are sufficiently smooth. We propose to reconstruct such missing fluctuations by iteratively applying a spherical harmonic expansion to fluctuations in the unmasked region. The accuracy of reconstruction depends on the mask geometries, the spectrum of underlying density fluctuations, and the number of iterations. For Gaussian fluctuations with the Harrison-Zel'dovich spectrum, our method provides more accurate restoration than naive methods using the brute-forth matrix inversion or the singular value decomposition.

I. INTRODUCTION

After the first data release of the cosmic microwave background (CMB) temperature fluctuations observed by the Wilkinson Microwave Anisotropy Probe (WMAP), anomalous signatures in the CMB on large angular scales, so called "large-angle anomalies" have been claimed by many authors [1, 2, 3, 4, 5, 6, 7, 8, 9, 10, 11] and also confirmed recently by the Planck mission [12]. So far, the origin has been veiled in mystery. They may be due to (a) difference in a priori significance and a posteriori significance [13, 14, 15, 16] (b) incomplete subtraction of foreground emissions [17, 18, 19] (c) contribution from large scale structures via the integrated Sachs-Wolfe effect [12, 20, 21, 22, 23, 24, 25, 26, 27, 28], or kinetic Sunyaev-Zel'dovich effect [29], (d) possible systematics from instruments [30] (e) incomplete treatment of masking [31], or (f) extensions of inflationary models [32, 33, 34, 35, 36, 37, 38, 39].

In real observation, we cannot observe the whole sky with a sufficiently high signal-to-noise (S/N) ratio. A conservative approach is to mask out the region (e.g., the Zone of Avoidance), where the S/N ratio is low and just ignore the data on it.

For estimating the power spectrum of fluctuations in the sky, we can use deconvolution techniques [e.g. 40] assuming an isotropy prior on the power spectrum. However, for estimating the density field itself, we need to develop methods that can reconstruct the phases (if expressed in complex numbers) as well as the amplitudes of missing fluctuations.

In order to reconstruct missing data on the masked region, we need to find the inverse of the masking operator. However, in general, the masking matrix is singular thus not invertible. We need to assume a certain prior information about the underlying data such as isotropy and smoothness [31, 41, 42, 43] or their derivatives [44] in order to regularize the inverse operator. Since the result depends on the choice of the prior, the robustness of each reconstruction method should be mutually checked.

In this paper, we propose a new method for regularizing the inverse of masking operators using the iterative spherical harmonic expansion (IHE). As our aim is to probe the origin of the large-angle CMB anomalies, we ignore the effect of noise in the signal in the following, which is a good approximation for large-angle fluctuations.

This paper is organized as follows. In section II, we describe the formulation of our reconstruction method using the iterative spherical harmonic expansion and our simulations for random Gaussian fluctuations. In section III, we show the accuracy of the reconstruction, which depends on the pixelization of the sky, the underlying power spectrum, and the number of iteration. And then we compare the accuracy of our method to that of the brute-force and the singular value decomposition (SVD) method. In section IV, we give our conclusion.

II. ITERATIVE HARMONIC EXPANSION

A. Theory

Suppose a density field $\delta(\hat{\gamma})$ on a unit sphere where $\hat{\gamma}$ represents a unit vector that specifies the angular position in the sky. The observed field is given by

$$\delta_{\text{obs}}(\hat{\gamma}) = W(\hat{\gamma})\delta(\hat{\gamma}), \tag{1}$$

where $W = 0$ in the masked region and $W = 1$ elsewhere. Then we can obtain the pseudo harmonic coefficient $\tilde{a}_i$ by simply integrating over the whole sky,

$$\tilde{a}_i = \int d\Omega \, \delta(\hat{\gamma})W(\hat{\gamma})Y_i^*(\hat{\gamma}) \tag{2}$$

where $W_{ij} = \int d\Omega \, WY_jY_i^*$ is the (i, j) component of the mode coupling matrix due to incomplete sky coverage, $Y_i(\hat{\gamma})$ is a spherical harmonic, and $d\Omega$ is the surface element on a unit sphere. For simplicity, we use the single subscript index $i = \ell^2 + \ell + m + 1$ where ℓ and m represent a multipole moment and

[*]Electronic address: atsushi.nishizawa@ipmu.jp

(a) Original map with mask

(c) Pseudo-$a_{\ell m}$ reconstruction

(e) Pseudo-$a_{\ell m}$ residual

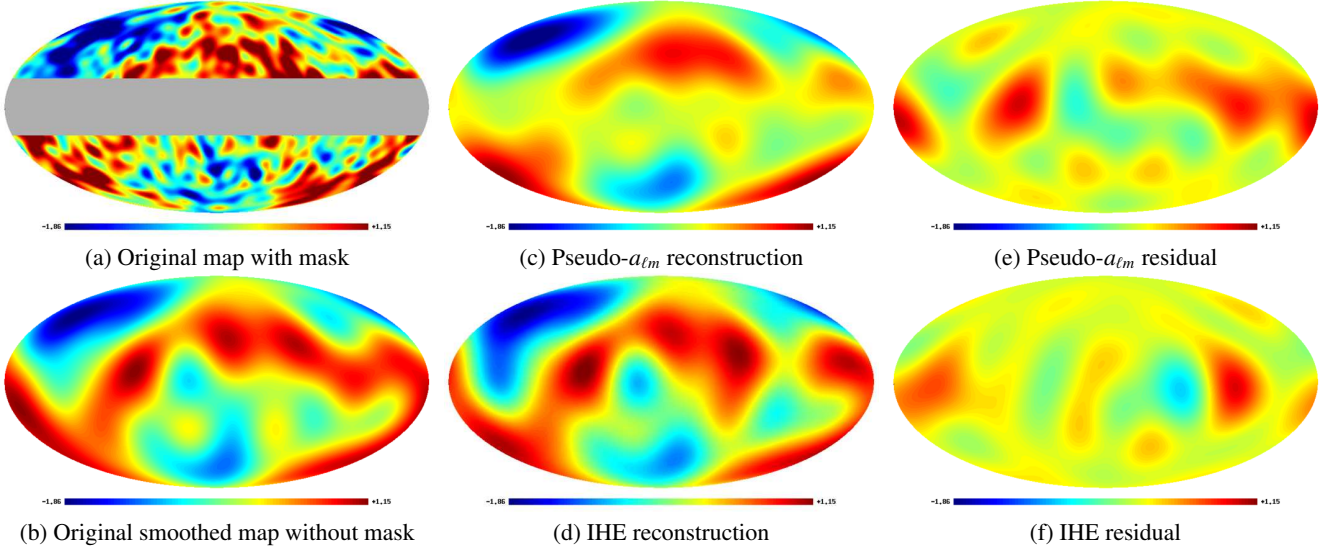(b) Original smoothed map without mask

(d) IHE reconstruction

(f) IHE residual

FIG. 1: Plots of an original and reconstructed maps. (a) Original simulated map with $\ell_{cut} = 30$ and a sky cut $|b| < 20°$, which is used as an input. (b) Original simulated map smoothed with $\ell_{cut} = 7$ on a full sky (no mask). (c) Reconstructed map with $\ell_{max} = 7$ using pseudo-a_i. (d) Reconstructed map with $\ell_{max} = 7$ using IHE with $N_{ite} = 10$ iterations. (e) Residual map after subtraction:(b)-(c). (f) Residual map after subtraction:(d)-(b). Color scale (-1.87 to 1.55) is the same for all the figures.

an azimuthal number, respectively. In terms of true harmonic coefficients to be reconstructed a_j^{true}, Eq. (2) can be written as

$$\tilde{a}_i = \sum_{j}^{\infty} a_j^{\text{true}} W_{ij}. \tag{3}$$

The mode coupling matrix W is explicitly given as [40]

$$
\begin{aligned}
W_{i_1 i_2} &= \sum_{i_3} w_{i_3} \int d\Omega\, Y_{i_3}^* Y_{i_2} Y_{i_1} \\
&= \sum_{i_3} w_{i_3} (-1)^{m_2} \left[\frac{(2\ell_1 + 1)(2\ell_2 + 1)(2\ell_3 + 1)}{4\pi} \right]^{1/2} \\
&\quad \times \begin{pmatrix} \ell_1 & \ell_2 & \ell_3 \\ 0 & 0 & 0 \end{pmatrix} \begin{pmatrix} \ell_1 & \ell_2 & \ell_3 \\ m_1 & -m_2 & m_3 \end{pmatrix},
\end{aligned} \tag{4}
$$

where $w_i = \int d\Omega\, W Y_i^*$ and $(:::)$ denotes the Wigner $3j$-symbols. Note that the subscript i_j depends only on ℓ_j and m_j, i.e. $i_j = \ell_j^2 + \ell_j + m_j + 1$.

As shown in Eq. (3), a_i^{true}'s can be obtained by inverting the mode coupling matrix W. However, in general, it can be singular and not invertible. In order to regularize the inversion, we propose the following iterative scheme. The iteration process starts from

$$\tilde{a}_i^{(1)} = \int d\Omega\, \delta(\hat{\gamma}) W(\hat{\gamma}) Y_i^*(\hat{\gamma}), \tag{5}$$

which we call "the pseudo-a_i's". For $m > 1$, the m-th set of $\tilde{a}_i$'s is constructed iteratively from two maps; the original observed map at the unmasked region and the map reconstructed from the inverse transform of the $(m-1)$-th $\tilde{a}_i$'s at the masked region,

$$\tilde{a}_i^{(m)} = \int d\Omega \left[\delta(\hat{\gamma}) W(\hat{\gamma}) + \tilde{\delta}^{(m-1)}(\hat{\gamma}) S(\hat{\gamma}) \right] Y_i^*(\hat{\gamma}), \tag{6}$$

where

$$\tilde{\delta}^{(m-1)}(\hat{\gamma}) = \begin{cases} \sum_{i}^{\infty} \tilde{a}_i^{(m-1)} Y_i(\hat{\gamma}) & m \geq 2, \\ 0 & m = 1, \end{cases} \tag{7}$$

and $S = 1 - W$. In what follows, we assume that fluctuations whose angular scales are larger than that of the masked region do not significantly correlate with fluctuations smaller than the masked region. In that case, the summation in Eq. (3) and Eq. (7) can be truncated at a certain multipole i_{max} as long as we concern large-angle fluctuations corresponding to multipoles $i \ll i_{max}$. In what follows, we sum up a_i's up to the multipole i_{imax}, and we omit the summation symbol when no confusion arises.

Substituting Eq. (7) into (6) recursively, we obtain the general formula of the m-th iterated harmonic coefficients as a series of S_{ij},

$$\tilde{a}_i^{(m)} = \tilde{a}_j^{(1)} (\delta_{ij}^K + S_{ij} + S_{ik} S_{kj} + \cdots + [S^{m-1}]_{ij}), \tag{8}$$

where δ_{ij}^K is the Kronecker delta, and $S_{ij} = \delta_{ij}^K - W_{ij}$. The map between m-th iterated harmonic coefficient $\tilde{a}_i^{(m)}$ is equivalent to the product of $\tilde{a}_i^{(1)}$'s and the Taylor expansion of the inverse of the mode coupling matrix W truncated at the $(m-1)$-th order,

$$\tilde{a}_i^{(m)} \simeq \tilde{a}_j^{(1)} [(\delta^K - S)^{-1}]_{ij} = \tilde{a}_j^{(1)} [W^{-1}]_{ij}, \tag{9}$$

Thus $\tilde{a}_i^{(m)}$'s approximately represent fluctuations in which the mode coupling matrix W is deconvolved. The number of iteration N_{ite} should be evaluated using Monte-Carlo simulations, which is discussed later in Sec.III.

We can regard the above process as a mapping from a observable to the estimator,

$$F_{\text{IHE}} : \tilde{a}_i \rightarrow \tilde{a}^{(m)}. \quad (10)$$

As we will see in Sec. III, the accuracy of the IHE method depends on the maximum multipole ℓ_{max} to be reconstructed, the spectrum of the underlying field δ, the mask geometry, and the number of iteration N_{ite}. Thus we can write $F_{\text{IHE}} = F_{\text{IHE}}(\ell_{\text{max}}, \delta, W, N_{\text{ite}})$.

Note that the computation time for estimating $\tilde{a}^{(N_{\text{ite}})}$ can be significantly reduced if we use Eq. (6) instead of Eq. (8). The reason is as follows. As the rank of the matrix S_{ij} is of the order ℓ_{max}^2, it costs $N_{\text{pix}}\ell_{\text{max}}^4$ by Eq. (4), and matrix algebra of Eq. (8) costs $\sim N_{\text{ite}}\ell_{\text{max}}^6$ computations. If one uses Eq. (6), it would be of the order $N_{\text{ite}}N_{\text{pix}}\ell_{\text{max}}^2$, where N_{ite} is the number of iteration, and N_{pix} is the number of pixels which tile the sky, and ℓ_{max} is the maximum multipole to be reconstructed. For example, for given $\ell_{\text{max}} = 10$, $N_{\text{pix}} = 12 \times 1024^2$ pixels and 5 time iteration, the computation time will be reduced by a factor of ~ 25.

B. Simulation

In order to assess the accuracy of reconstruction, we generate 1000 random isotropic Gaussian density fields in the sky. We use the code *synfast*, which is publicly available as a package in Healpix [50] [45] for generating random Gaussian maps. First, we use the Harrison-Zel'dovich spectrum as the input power spectrum. It gives an angular power spectrum $C_\ell \propto l^n$ where $n = -2$ on large angular scales, in the Einstein de-Sitter universe which correspond to the Sachs-Wolfe plateau of the CMB power spectrum. As a simple model of the zone of avoidance, we consider an azimuthally symmetric mask $W(\hat{\gamma}) = 0$ at the Galactic latitude b smaller than 20 degrees, i.e. $|b| < 20°$ and $W = 1$ otherwise. We use pixels that are sufficiently smaller than the size of the mask and the fluctuation scales to be reconstructed in order to reduce the errors due to the pixelization effect (see Sec. III A). We adopt the Healpix resolution $N_{\text{side}} = 512$ (the total number of pixels on the whole sky is $N_{\text{pix}} = 12 \times N_{\text{side}}^2 = 3145728$). The input power spectrum should be truncated at sufficiently small scales ℓ_{cut} compared to the scale to be reconstructed ℓ_{max}, i.e. $\ell_{\text{max}} \ll \ell_{\text{cut}}$. The cut-off scale ℓ_{cut} is inferred from the detector resolution scale in CMB observations or the shot noise dominant scales in galaxy surveys. In our simulated maps, we set $\ell_{\text{cut}} = 30$, which is sufficiently smaller than the claimed anomalous multipoles in the CMB. We find that the choice of ℓ_{cut} is not sensitive to our result.

III. RESULT

In this section, we first explore the pixelization effect, which may affect the accuracy of reconstruction in Sec. III A and then we compare our reconstruction method with other inversion methods using the brute-force or the singular value
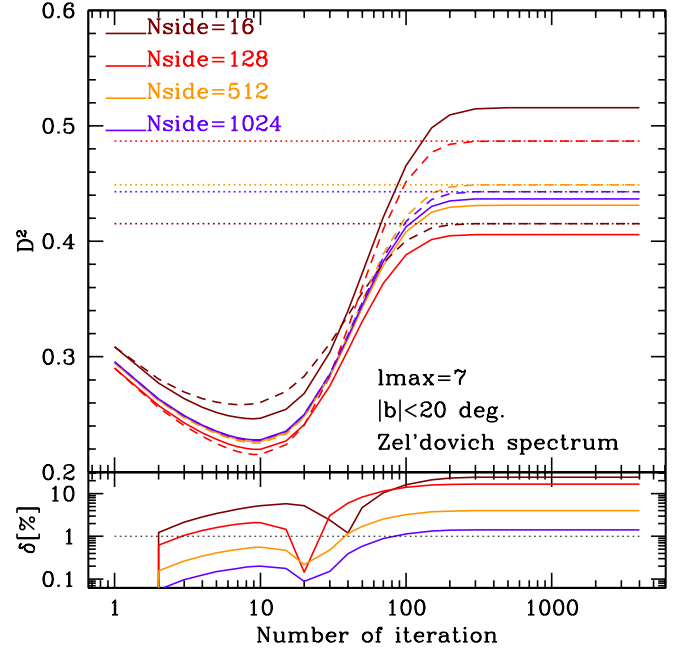

FIG. 2: The accuracy of map reconstruction averaged over 1000 realizations of Gaussian maps as a function of the iteration number for a mask $|b| < 20°$ with $\ell_{\text{max}} = 7$ for various pixel resolution N_{side}. Both solid and dashed lines are obtained by using Eqs. (6) and (7). Dashed lines represent values for which approximated S_{ij}'s for pixel-based masks are used. Solid lines show values for which the exact expression of Eq. (11) is used. Dotted lines indicate values obtained by using the direct inversion of the mode coupling matrix W, the second equation in Eq. (9). In the bottom panel, we show the relative differences of the accuracy in percentage. $N_{\text{side}} = 1024$ provides accuracy better than a few percent. $N_{\text{ite}} \sim 10$ with $N_{\text{side}} = 512$ can achieve sub-percent accuracy.

decomposition (SVD) in Sec. III B. Finally, we discuss the condition of the original maps that can be reconstructed by using the IHE in Sec. III C.

A. Pixelization effect

We need to assess the accuracy of the mode coupling matrix W since it may be close to being singular. In other words, the difference between $W(\hat{\gamma})$ and $W(\hat{\gamma}_i)$ should be carefully checked where $\hat{\gamma}$ and $\hat{\gamma}_i$ are unpixelized and pixelized positions on a unit sphere, respectively. In order to do so, we need to estimate uncertainties due to pixelization of the sky as it could be potential sources of errors. For an azimuthally symmetric mask $W = 0$ for $|b| \leq b_0$, we do not need pixelization, since W_{ij} can be analytically calculated as

$$W_{ij} = 2\pi \left(1 - \int_{\pi/2-b_0}^{\pi/2+b_0} Y_i(\theta, 0) Y_j(\theta, 0) \sin\theta d\theta\right), \quad (11)$$

where θ is the polar angle, and $\theta = \pi/2 - b$. We compare the eigenvalues of W obtained by using Eq. (4) and Eq. (11) to study the accuracy of the calculated matrix. The differ-

ence depends on the resolution of pixels N_{side}. We adopt $N_{side} = 16, 128, 512, 1024$ and find that the differences in the eigenvalues are less than 0.01% for $N_{side} \geq 512$. In order to evaluate the accuracy of map reconstruction, we use the L^2 norm of the fractional difference between the reconstructed map and the original map,

$$D_\ell^2 \equiv \frac{\sum_i^{Npix}[\delta_{rec}(\hat{\gamma}_i; \ell) - \delta_{true}(\hat{\gamma}_i; \ell)]^2}{\sum_i^{Npix} \delta_{true}^2(\hat{\gamma}_i; \ell)} \qquad (12)$$

where δ_{rec} and δ_{true} describe the reconstructed and the original density fluctuations contributed from the ℓ-th multipole mode,

$$\delta(\hat{\gamma}; \ell) \equiv \sum_{m=-\ell}^{\ell} a_{\ell m} Y_{\ell m}(\hat{\gamma}), \qquad (13)$$

respectively. An overall fractional difference D^2 is defined by substituting $\delta(\hat{\gamma})$ for $\delta(\hat{\gamma}, \ell)$ in Eq. (12) where $\delta(\hat{\gamma})$ is a sum of all the multipole contributions, i.e. $\delta(\hat{\gamma}) = \sum_\ell \delta(\hat{\gamma}; \ell)$.

In Fig. 2, we can see the difference between a pixelized mask and an unpixelized "smooth" mask given by Eq. (11). Using Healpix, we pixelize the mask with different resolution N_{side} where the total number of pixel on the sky is defined as $N_{pix} = 12 \times N_{side}^2$. Before looking into the pixelization effect, we first study the overall behaviour of reconstruction accuracy as a function of the number of iteration. As we increase the number of iteration, the accuracy of reconstruction gradually improves at $N_{ite} < 10$ then it begins to degrade. Finally, the D^2 accuracy converges to the one obtained by using the brute-force inversion (dotted lines in the Fig. 2). As we can see in the bottom panel of Fig. 2, the differences in D^2 between the pixelized and unpixelized W_{ij} are significant for $N_{side} = 16$ and 128, while they are less than 1% at the D^2 minimum for $N_{side} \geq 512$. We then conclude that the pixelization effect can be ignored when we use sufficiently fine pixels with $N_{side} \geq 512$.

B. Comparison with W^{-1} and SVD

Using Eq. (9), we can compare our method to the direct brute-force inversion of the matrix W and the singular value decomposition[46].

If the mode coupling matrix W is invertible, we obtain the unique solution of the underlying density fluctuation within the mask. However, if the matrix W contains some eigenvalues which are close to zero, where the matrix is close to being singular, the inversion causes big errors. In such a case, we can remove the singularity by replacing the small eigenvalues with zero, so called the SVD method. More specifically, the matrix W can be decomposed into three matrices as,

$$W = U \, \Sigma \, V^\dagger, \qquad (14)$$

where V and U are $i_{max} \times i_{max}$ unitary matrices and a superscript $\dagger$ denotes the Hermitian conjugate. Σ is the diagonal matrix which consists of the eigenvalues of W, or called as the singular values. The order of the eigenvalues in Σ is arbitrary
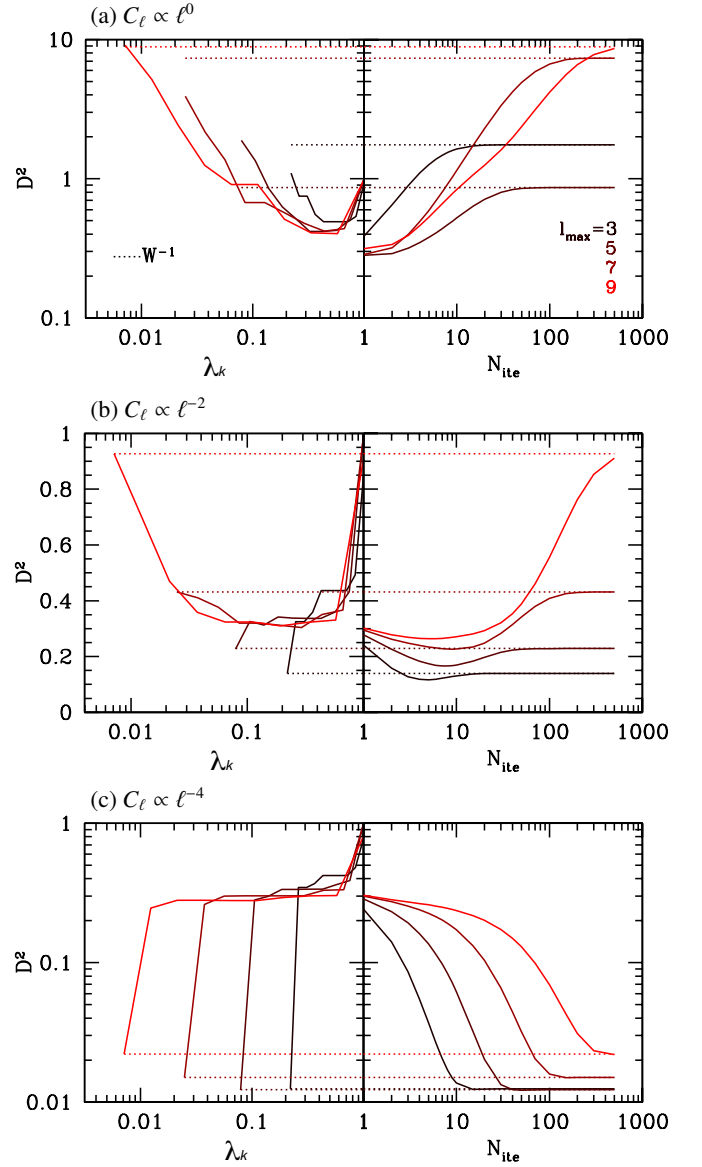

FIG. 3: In the right panels, we plot D^2 accuracy as a function of iteration number. Three different rows show the different underlying density fluctuations that have power-law spectrum of $C_\ell \propto \ell^0$, ℓ^{-2} and ℓ^{-4} from top to bottom. For a red ($n = 0$) spectrum, we do not see any improvement. However, for a flat ($n = -2$) spectrum, there exists an optimal number of iteration around $N_{ite} = 10$ that minimizes D^2. The optimal N_{ite} depends on the ℓ_{max}. For a blue ($n = -4$) spectrum, D^2 converges to a few percent accuracy after sufficient number of iteration. For all cases, after a sufficient number of iteration, D^2 converges to the value which is obtained by the direct inversion. In the left panels, we show the result for the SVD method for the comparison as a function of eigenvalue threshold λ_k.

but they are arranged in a descending order so that the decomposition is determined uniquely. Let the k−th eigenvalue be λ_k, and the eigenvalues smaller than λ_k are set to zero. Then the pseudo inversion of W is written in terms of Σ^+, the rank-k diagonal matrix that consists of the reciprocal of the non-zero
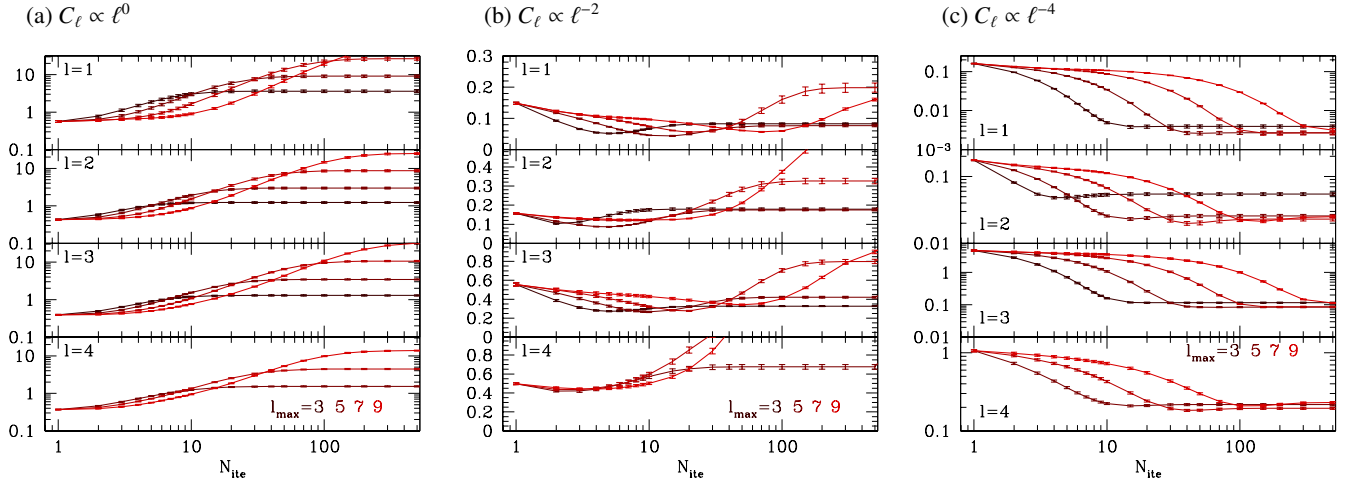
FIG. 4: The IHE reconstruction accuracy D_ℓ^2 for each multipole component. From right to left, the indices of underlying power spectrum are $n = 0, -2$ and -4, respectively. From top to bottom, the components of multipoles $\ell = 1$ to 4 are shown. We reconstruct the masked map with maximum multipoles of $\ell_{max} = 3, 5, 7$ and 9. The error bars represent 1 σ standard deviation calculated from 1000 random realizations.

eigenvalues that are equal to or larger than λ_k, as

$$W^+ = V \, \Sigma^+ \, U^\dagger, \qquad (15)$$

which gives

$$a_i^{est} = \tilde{a}_j W_{ij}^+. \qquad (16)$$

The choice of threshold λ_k is not trivial, and should be carefully determined *a priori* because the mapping F_{SVD} depends on various factors including the threshold λ_k: i.e. $F_{SVD} = F_{SVD}(\ell_{max}, \delta, W, \lambda_k)$. In this context, the *singularity* can only be defined in terms of λ_k. More specifically, the mapping F_{SVD} is contaminated by the eigenvalues which are close to being *singular* if $\partial D^2/\partial \lambda_k < 0$. In such cases, the threshold of eigenvalues should be increased to implement more accurate reconstruction. The brute-force inversion corresponds to $F_{inv} = F_{SVD}(\ell_{max}, \delta, W, \lambda_k = 0)$.

In the left panels of Fig. 3, D^2 is shown as a function of the minimum non-zero eigenvalue λ_k. The solid lines show the different maximum multipole to be reconstructed, $\ell_{max} = 3, 5, 7, 9$ from dark to light color. The different three rows show the different power of the input power spectra which will be discussed in detail in the next section. Let us focus on the middle panel. For $\ell_{max} = 3$ and 5, D^2 increases monotonically as we increase the threshold. It means that the F_{SVD} is not contaminated by singular eigenvalues as $\partial D^2/\partial \lambda_k > 0$. On the other hand, for $\ell_{max} = 7$ and 9, D^2 has a minimum around $\lambda_k \sim 0.1$. Thus the eigenvalues smaller than ~ 0.1 may be the contaminant of the mapping F and we can better estimate the original density fluctuations when we limit the eigenvalues as $\lambda < 0.1$. In the right panel of Fig. 3, we show D^2 for our IHE method as a function of the number of iteration. As in Fig. 2, D^2 has the minimum around $N_{ite} \simeq 10$ depending on the maximum multipole. After a sufficient number of iteration, D^2 values converge to those obtained by using the brute-force inversion, which are shown as the horizontal dashed lines in

Fig.2. Our IHE method with a certain finite number of iteration is always better than the SVD method. However, in practice, we should know a priori the optimal number of iteration. The number depends on the mask geometry, the maximum multipole to be reconstructed, and the underlying spectrum of the density fluctuation. We can estimate the optimal iteration number by carrying out Monte-Carlo simulations. In the next section we will see how the result changes for different types of underlying power spectrum.

C. Dependence on underlying power spectrum

Reconstruction accuracy depends on the underlying power spectrum $C_\ell \propto \ell^n$ of the fluctuation as each harmonic mode is not independent in the masked incomplete sky even the underlying fluctuation is Gaussian. We consider three power law indices, $n = 0, -2$ and -4, which correspond to the following three cases. The projected two dimensional galaxy or dark matter distribution is approximated as $C_\ell^g \propto \ell^0$ [e.g. 47] on large scales, and the ordinary Sachs-Wolfe spectrum is approximated as $C_\ell^{SW} \propto \ell^{-2}$ [48]. On very large-angular scales, the integrated Sachs-Wolfe effect, which gives $C_\ell^{iSW} \propto \ell^{-4}$ [e.g. 49] dominates the CMB in the standard ΛCDM scenario.

Given the typical scale of mask θ_M, it is impossible to reconstruct the fluctuation whose scale is smaller than $\ell_M \geq 180/\theta_M$. Because of the mode coupling, fluctuations with angular scales corresponding to ℓ_M are strongly affected by fluctuations with smaller angular sizes. If the spectral index is negative, the amplitude of a smaller scale fluctuation is weak and does not strongly disturb the large scale fluctuations. Thus the deconvolution mapping F is less affected by singularities. However, if the slope of the spectrum is flat or positive, large scale modes are highly contaminated by the noisy small scale fluctuations.

In Fig. 3, the top and bottom panels show D^2 accuracy for $n = 0$ and $n = -4$. For $n = 0$ case, the SVD has a min-

imum at $\lambda_k \sim 0.5$ that is larger than the case of $n = -2$. It means that $F_{\text{SVD}}(n = 0)$ is more affected by singularities than $F_{\text{SVD}}(n = -2)$. The IHE result in the right panels shows $N_{\text{ite}} = 1$ gives the best accuracy and it gradually degrades to the value given by the brute-force method. On the other hand, $F_{\text{SVD}}(n = -4)$ is not affected by singularities because it always shows $\partial D^2/\partial \lambda_k < 0$ for the SVD method. In Fig. 4, we also show the reconstruction accuracy for each multipole component, D_ℓ^2. The behaviour is similar to the one described in Fig. 3. The reconstruction accuracy is always better for low multipoles and that the optimal number of iteration depends also on the multipole component we are going to reconstruct.

IV. SUMMARY

We have developed a new method based on the iterative harmonic expansions (IHE) for reconstructing the missing fluctuations in the masked region in the sky. Reconstructing the data at a masked region is known as an inverse problem. Our method is equivalent to the brute-force inversion in the limit that the iteration number goes to infinity. However, in some cases, the finite truncation of the iteration gives a better estimate of the underlying fluctuation. The reconstruction accuracy depends on the geometrical shape of the mask, the maximum multipole mode to be included in the IHE analysis, the tilt of the underlying power spectrum, and the multipole component of the map to be reconstructed.

As an example, we have applied the method to reconstruct the missing data on an azimuthally symmetric mask. We have considered three types of gaussian fluctuations with the power-law indices $n = 0, -2$ and -4, which correspond to the galaxy power spectrum, the ordinary Sachs-Wolfe spectrum, and the integrated Sachs-Wolfe spectrum, respectively. For $n = -2$ case, we have found that there exists an optimal finite number of iteration that makes the reconstruction more accurate than the SVD method or the brute-force method. For $n = 0$ case, the pseudo-$a_{\ell m}$ is the best estimator for the projected density fluctuations. For $n = -4$ case, the brute-force inversion method gives the best accuracy. In that case, the IHE method can help to reduce the computation time of inversion.

It would be interesting to see how the significance of the large-angle CMB anomaly changes when we use different methods of map reconstruction. The IHE method may help to unveil the origin of the CMB anomaly. We will explore this problem in our future work.

[1] J. P. Ralston and P. Jain, International Journal of Modern Physics D **13**, 1857 (2004), arXiv:astro-ph/0311430.

[2] A. de Oliveira-Costa, M. Tegmark, M. Zaldarriaga, and A. Hamilton, Phys. Rev. D **69**, 063516 (2004), arXiv:astro-ph/0307282.

[3] F. K. Hansen, A. J. Banday, and K. M. Górski, MNRAS **354**, 641 (2004), arXiv:astro-ph/0404206.

[4] A. Hajian, T. Souradeep, and N. Cornish, ApJL **618**, L63 (2005), arXiv:astro-ph/0406354.

[5] J. W. Moffat, JCAP **10**, 012 (2005), arXiv:astro-ph/0502110.

[6] K. Land and J. Magueijo, MNRAS **367**, 1714 (2006), arXiv:astro-ph/0509752.

[7] A. Bernui, T. Villela, C. A. Wuensche, R. Leonardi, and I. Ferreira, Astronomy & Astrophysics **454**, 409 (2006), arXiv:astro-ph/0601593.

[8] C. J. Copi, D. Huterer, D. J. Schwarz, and G. D. Starkman, Phys. Rev. D **75**, 023507 (2007), arXiv:astro-ph/0605135.

[9] H. K. Eriksen, A. J. Banday, K. M. Górski, F. K. Hansen, and P. B. Lilje, ApJL **660**, L81 (2007), arXiv:astro-ph/0701089.

[10] C. Monteserín, R. B. Barreiro, P. Vielva, E. Martínez-González, M. P. Hobson, and A. N. Lasenby, MNRAS **387**, 209 (2008), 0706.4289.

[11] P. K. Samal, R. Saha, P. Jain, and J. P. Ralston, MNRAS **396**, 511 (2009), 0811.1639.

[12] Planck Collaboration, P. A. R. Ade, N. Aghanim, C. Armitage-Caplan, M. Arnaud, M. Ashdown, F. Atrio-Barandela, J. Aumont, C. Baccigalupi, A. J. Banday, et al., ArXiv e-prints (2013), 1303.5083.

[13] R. Aurich, S. Lustig, and F. Steiner, Classical and Quantum Gravity **27**, 095009 (2010), 0903.3133.

[14] A. Pontzen and H. V. Peiris, Phys. Rev. D **81**, 103008 (2010), 1004.2706.

[15] G. Efstathiou, Y.-Z. Ma, and D. Hanson, MNRAS **407**, 2530 (2010), 0911.5399.

[16] C. L. Bennett, R. S. Hill, G. Hinshaw, D. Larson, K. M. Smith, J. Dunkley, B. Gold, M. Halpern, N. Jarosik, A. Kogut, et al., ApJS **192**, 17 (2011), 1001.4758.

[17] L. R. Abramo, L. Sodré, Jr., and C. A. Wuensche, Phys. Rev. D **74**, 083515 (2006), arXiv:astro-ph/0605269.

[18] M. Cruz, P. Vielva, E. Martínez-González, and R. B. Barreiro, MNRAS **412**, 2383 (2011), 1005.1264.

[19] M. Hansen, J. Kim, A. M. Frejsel, S. Ramazanov, P. Naselsky, W. Zhao, and C. Burigana, JCAP **10**, 059 (2012), 1206.6981.

[20] K. T. Inoue and J. Silk, Astrophys. J. **648**, 23 (2006), arXiv:astro-ph/0602478.

[21] K. T. Inoue and J. Silk, Astrophys. J. **664**, 650 (2007), arXiv:astro-ph/0612347.

[22] A. Rassat, K. Land, O. Lahav, and F. B. Abdalla, MNRAS **377**, 1085 (2007), arXiv:astro-ph/0610911.

[23] N. Afshordi, G. Geshnizjani, and J. Khoury, JCAP **8**, 030 (2009), 0812.2244.

[24] C. L. Francis and J. A. Peacock, MNRAS **406**, 14 (2010), 0909.2495.

[25] A. Rassat, J.-L. Starck, and F.-X. Dupe, ArXiv e-prints (2013), 1303.4727.

[26] K. Tomita and K. T. Inoue, Phys. Rev. D **77**, 103522 (2008),

0712.1291.

[27] N. Sakai and K. T. Inoue, Phys. Rev. D **78**, 063510 (2008), 0805.3446.

[28] K. T. Inoue, MNRAS **421**, 2731 (2012), 1109.4527.

[29] H. V. Peiris and T. L. Smith, Phys. Rev. D **81**, 123517 (2010), 1002.0836.

[30] D. Hanson, A. Lewis, and A. Challinor, Phys. Rev. D **81**, 103003 (2010), 1003.0198.

[31] J. Kim, P. Naselsky, and N. Mandolesi, ApJL **750**, L9 (2012), 1202.0188.

[32] R. Aurich, S. Lustig, F. Steiner, and H. Then, Classical and Quantum Gravity **24**, 1879 (2007), arXiv:astro-ph/0612308.

[33] A. Emir Gümrükçüoglu, C. R. Contaldi, and M. Peloso, JCAP **11**, 005 (2007), 0707.4179.

[34] D. C. Rodrigues, Phys. Rev. D **77**, 023534 (2008), 0708.1168.

[35] A. Bernui and W. S. Hipólito-Ricaldi, MNRAS **389**, 1453 (2008), 0807.1076.

[36] M. Cruz, E. Martínez-González, P. Vielva, J. M. Diego, M. Hobson, and N. Turok, MNRAS **390**, 913 (2008), 0804.2904.

[37] A. Fialkov, N. Itzhaki, and E. D. Kovetz, JCAP **2**, 004 (2010), 0911.2100.

[38] H. Zheng and E. F. Bunn, Phys. Rev. D **82**, 063533 (2010), 1003.5548.

[39] H. Liu, A. M. Frejsel, and P. Naselsky, ArXiv e-prints (2013),

[40] E. Hivon, K. M. Górski, C. B. Netterfield, B. P. Crill, S. Prunet, and F. Hansen, Astrophys. J. **567**, 2 (2002).

[41] P. Abrial, Y. Moudden, J.-L. Starck, J. Fadili, J. Delabrouille, and M. K. Nguyen, Statistical Methodology **5**, 289 (2008), 0804.1295.

[42] M. Bucher and T. Louis, MNRAS **424**, 1694 (2012), 1109.0286.

[43] J.-L. Starck, M. J. Fadili, and A. Rassat, Astronomy & Astrophysics **550**, A15 (2013), 1210.6587.

[44] K. T. Inoue, P. Cabella, and E. Komatsu, Phys. Rev. D **77**, 123539 (2008), 0804.0527.

[45] K. M. Górski, E. Hivon, A. J. Banday, B. D. Wandelt, F. K. Hansen, M. Reinecke, and M. Bartelmann, Astrophys. J. **622**, 759 (2005).

[46] G. Efstathiou, MNRAS **348**, 885 (2004), arXiv:astro-ph/0310207.

[47] W. J. Frith, P. J. Outram, and T. Shanks, MNRAS **364**, 593 (2005), arXiv:astro-ph/0507215.

[48] R. K. Sachs and A. M. Wolfe, Astrophys. J. **147**, 73 (1967).

[49] A. Cooray, Phys. Rev. D **65**, 083518 (2002), arXiv:astro-ph/0109162.

[50] http://healpix.jpl.nasa.gov/